

NUMERICAL MODELING OF COLLECTIVE EFFECTS IN FREE ELECTRON LASER

Igor Zagorodnov, DESY, Hamburg, Germany

Abstract

In order to have a free electron laser (FEL) of high performance we need to design and optimize it taking into account the dynamics of electrons and their interactions with each other and with their surroundings. An accurate self-consistent simulation of collective effects in the charged beams remains a challenging problem for numerical analysis. In this paper we consider only the modeling of FEL process in an undulator section. We give a short overview of the numerical methods adopted in different FEL codes. Advantages and drawbacks of these methods will be discussed. Some approaches to improve the accuracy and efficiency of the codes will be presented and the remaining challenges in FEL modeling will be highlighted.

INTRODUCTION

An accurate self consistent simulation of collective effects in the charged beams remains a challenging problem for numerical analysis. During the last decades several numerical codes have been developed to model the non-linear process in a self-amplified spontaneous emission (SASE) free electron lasers (FEL). In this paper we review the mathematical FEL model used in these codes [1-4]. To illustrate the numerical methods we use those implemented in code ALICE [5].

Modelling of the FEL is challenging due to different scales of the process [6]. The disparity of scales up to 12 orders of magnitude imposes several limitations on the size of the systems that can be modelled on the basis of classical Maxwell-Vlasov set of equations.

In order to be able to study the FEL process two main approximations are used: wiggler-period averaging of the equations of motion and slowly-varying envelope approximation of the Maxwell equations.

FEL MATHEMATICAL MODEL

We consider the case of helical undulator with the magnetic field on the axis given by

$$\vec{B}_\perp^w = (\nabla \times \vec{A}_\perp^w)_\perp = \frac{\partial}{\partial z} \begin{pmatrix} -A_y^w \\ A_x^w \end{pmatrix} = \frac{mc}{e} K k_w \begin{pmatrix} \cos(k_w z) \\ -\sin(k_w z) \end{pmatrix}.$$

Following the approach of [1] the equations of motion for helical undulator can be derived from Hamiltonian

$$h(\vec{r}_\perp, ct; \vec{P}_\perp, P_t; z) = -\gamma \left[1 - \frac{1 + |\vec{P}_\perp|^2 + |\vec{a}_\perp|^2 + 2(\vec{P}_\perp, \vec{a}_\perp)}{\gamma^2} \right]^{0.5} + a_z.$$

In order to avoid the necessity to resolve the fast "slalom" motion we carry out *wiggler-period averaging* of the Hamiltonian. The scalar product disappears and we obtain the averaged Hamiltonian

$$h(\vec{r}_\perp, ct; \vec{P}_\perp, P_t; z) = -\gamma \left[1 - \frac{1 + |\vec{P}_\perp|^2 + |\vec{a}_\perp|^2}{\gamma^2} \right]^{0.5} + a_z.$$

The squared module of the transverse part of the vector potential $\vec{a} = e\vec{A}/(mc)$ can be approximated as

$$|\vec{a}_\perp|^2 = K^2 + 2a_s K \sin(\psi + \varphi_s).$$

Here $\psi = (k + k_w)z - \omega t$ is a particle phase, K is an undulator parameter, $a_s \exp(i\varphi_s)$ is a normalized complex amplitude of the amplified wave

$$A_x + iA_y = -imc e^{-1} a_s e^{i(kz - \omega t + \varphi_s)},$$

$$\vec{E}_\perp = -\frac{\partial}{\partial t} \vec{A}.$$

The canonical moments are defined by relations

$$\vec{P}_\perp = \gamma \frac{d\vec{r}_\perp}{dz} \beta_z - \vec{a}_\perp, \quad P_t = -\gamma + \frac{e}{mc^2} \varphi.$$

The equations of motion derived from the averaged Hamiltonian read

$$\frac{d\psi}{dz} = k_w - k(2\gamma^2)^{-1} \left(1 + |\vec{P}_\perp|^2 + K^2 \right),$$

$$\frac{d\gamma}{dz} = \frac{eK}{mc^2 \gamma^2} \Re(\tilde{E} e^{i\psi}) - \frac{e}{mc^2} E_z,$$

$$\frac{d\vec{r}_\perp}{dz} = \frac{\vec{P}_\perp}{\gamma \beta_z},$$

$$\frac{dP_x}{dz} = -\left(\frac{K^2 k_x^2}{\gamma \beta_z} + \frac{eg}{mc} \right) x, \quad \frac{dP_y}{dz} = -\left(\frac{K^2 k_y^2}{\gamma \beta_z} - \frac{eg}{mc} \right) y,$$

where $g = \partial_y B_x$ describes the gradients of the focusing quadrupole lattice and we have used the following representations of the undulator parameter and the transverse EM field

$$K(x, y, z) = K_0(x, y, z) \left(1 + \frac{k_x^2}{2} x^2 + \frac{k_y^2}{2} y^2 \right),$$

$$E_\perp = E_x + iE_y = \tilde{E}(\vec{r}, t) e^{i(kz - \omega t)} + c.c.$$

We split the electromagnetic field in the transverse and the longitudinal components. The longitudinal electrostatic field comes from the bunching and can be suggested to be a nearly periodic one. Then the Fourier components of the longitudinal field can be found from the equation [1]

$$\left(\nabla_\perp^2 - \frac{n^2(k + k_w)^2}{\gamma_z^2} \right) E_z^{(n)} = \frac{in(k + k_w)}{\epsilon_0 \gamma_z^2} \rho^{(n)},$$

$$\rho^{(n)}(\vec{r}_\perp) = \frac{1}{2\pi} \int_0^{2\pi} \rho(\vec{r}_\perp, \psi) e^{-in\psi} d\psi = -\frac{I}{Nv_z} \sum_{i=1}^N e^{-in\psi_i} \delta(\vec{r}_\perp - \vec{r}_{i\perp}).$$

The transverse field is written in the complex form with amplitude $\tilde{E}(\vec{r}, t)$ which fulfils the parabolic equation (paraxial or *slowly-varying envelope approximation*)

$$\left[\nabla_{\perp}^2 + 2ik \left(\frac{\partial}{\partial z} + \frac{1}{c} \frac{\partial}{\partial t} \right) \right] \tilde{E}(z, t) = ikc\mu_0 \frac{K}{\gamma} v_z \rho^{(1)}(z, t).$$

Along the trajectory $t = t_0 + z/c$ this equation can be rewritten in a simpler form

$$\left[\nabla_{\perp}^2 + 2ik \frac{d}{dz} \right] \tilde{E} \left(z, t_0 + \frac{z}{c} \right) = ikc\mu_0 \frac{K}{\gamma} v_z \rho^{(1)} \left(z, t_0 + \frac{z}{c} \right).$$

If the Pierce parameter [7] $\rho = c\gamma_z^2 \Gamma \omega^{-1}$ is small and the transverse variation of the longitudinal field can be neglected than the following set of normalized and simplified equations can be considered

$$\hat{x}'' = -(\hat{k}_x^2 + \hat{g})\hat{x}, \hat{y}'' = -(\hat{k}_y^2 - \hat{g})\hat{y},$$

$$\frac{d\psi}{d\hat{z}} = \hat{C} + \hat{\eta} - \frac{B}{2}(\hat{x}'^2 + \hat{y}'^2), \frac{d\hat{\eta}}{d\hat{z}} = |\hat{u}| \cos(\psi + \psi_r) - \hat{E}_z,$$

$$\hat{E}_z = \hat{E}_z^{(0)} - \hat{\Lambda}_p^2 \frac{1}{N_{jk}} \sum_{i=1}^{N_{jk}} [\pi \operatorname{sgn}(\psi - \psi_i) - (\psi - \psi_i)],$$

$$\left[\frac{1}{2iB} \hat{\Delta}_{\perp} + \frac{d}{d\hat{z}} \right] \hat{u} \left(\hat{r}_{\perp}, \hat{z}, \tau_0 + \frac{\hat{z}}{c} \right) = -2a^{(1)} \left(\hat{r}_{\perp}, \hat{z}, \tau_0 + \frac{\hat{z}}{c} \right),$$

where $\hat{x} = xr_0^{-1}$, $\hat{y} = yr_0^{-1}$, ($r_0 = \sqrt{2\sigma_x\sigma_y}$) are transverse particle coordinates, $\hat{\eta} = (\gamma - \gamma_0)(\gamma_0\rho)^{-1}$ is an energy deviation, \hat{C} is a detuning parameter, \hat{u} is the normalized (in complex notation) electric field and \hat{E}_z is the longitudinal electric field. The other parameters in Eq. (1) are defined as in [7, Chapter I].

NUMERICAL METHODS

In last decades several FEL codes have been developed around the world. In our studies at DESY we use mainly three codes whose basic features are listed in Table 1.

Table 1: Numerical Methods in Different Codes

	FAST[2]	Genesis 1.3[3]	ALICE[5]
Equations of motion	Runge-Kutta	Runge-Kutta	Leap-frog
EM field solver	Integral representation	Finite-difference, ADI	Finite-difference, Neumann
Boundary condition	Free space	Dirichlet	Free space with PML

These codes are based on the mathematical model described in the previous section. In the following we consider the numerical methods implemented in code ALICE [5]. In this code the equations of motion of the particles are integrated with symplectic “leap-frog” scheme. The parabolic field equation is resolved with implicit Neumann finite difference scheme based on azimuthal expansion. Additionally we have implemented

the open boundary condition with the help of perfectly matched layer (PML) for parabolic equation. The last feature allows for a mesh only in the bunch vicinity. The implemented field solver is accurate and fast. The code is parallelized and allows to use one dimensional, rotationally symmetric or fully three dimensional models.

Particle Distribution

At the beginning we divide the bunch longitudinally in N_s slices (numerated from the tail) with the length equal to the radiation wavelength. The initial particle distribution in the slice is generated with the “quiet start” method [8]. For this purpose we use the Sobol sequences [9]. The uniform distribution is converted to the Gaussian one with the help of the inverse error function

$$y = \sigma\sqrt{2} \operatorname{erf}^{-1}(2x-1) + \mu.$$

Figure 1 presents a comparison with the code Genesis 1.3 [3]. We carry out a simulation with only one slice in amplifier model. The space of parameters corresponds to SASE2 undulator at wavelength of 0.1 nm as described in [10]. The left plot compares the radiation power at saturation. The first comparison was done in the January 2008 [11] (version 1.0 of Genesis 1.3). The disagreement in the saturation power at the level of 20 % was obtained. After data analysis we have found that the used in Genesis 1.3 the “Box-Mueller” algorithm [9] (to convert the uniform distribution to Gaussian one) has spoiled the “quiet-start” property and the statistics of the particle distribution. The new version 2.0 of Genesis 1.3 released in April 2008 allows to use the inverse error function transformation (parameter inverfc=1). With this option results obtained by both codes converge together.

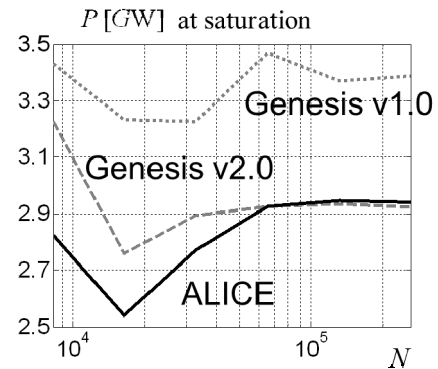


Figure 1: Convergence of the different codes.

The noise statistics in the slice is imposed following Fawley [12]. The n_p macroparticles in each beam slice are subdivided into an ensemble of n_b beamlets, each composed of $2M$ macroparticles (M is the order of the highest harmonic of interest). The $2M$ macroparticles in each beamlet k are loaded uniformly

$$\theta_{jk} = \theta_{0k} + (j-1) \frac{\pi}{M}, \quad j = 1..2M, k = 1..n_b,$$

where θ_{0k} is uniformly increased with index k over the interval $\left[0, \frac{\pi}{M}\right]$. To model the effects of shot noise a small random deviations,

$$\delta\theta_{jk} = \sum_{m=1}^{m=M} a_{mk} \cos(m\theta_{jk}) + b_{mk} \sin(m\theta_{jk}),$$

are added to the macroparticle positions. Each coefficient a_{mk}, b_{mk} are independently picked from Gaussian distributions with rms width

$$a_{mk,rms} = b_{mk,rms} = \sigma_{mk} = \frac{1}{m\sqrt{N_b}} \times \begin{cases} \sqrt{2}, & m < M, \\ 1, & m = M. \end{cases}$$

Note that for $m = M$ the rms width σ_{mk} is different from that given in [12]. Indeed, instead of Eq (5a) from [12] we obtain

$$\frac{1}{2M} \sum_{j=1}^{2M} \cos(m(\theta_{jk} + \delta\theta_{jk})) = \begin{cases} -\frac{m}{2} b_{mk}, & m < M, \\ -\frac{M}{2} (2b_{Mk} \sin^2(M\theta_{0k}) + a_{Mk} \sin(2M\theta_{0k})), & m = M. \end{cases}$$

For $m < M$ we have

$$\left\langle \left| \sum_{j=1}^{2M} \cos(m(\theta_j + \delta\theta_j)) \right|^2 \right\rangle = m^2 M^2 \sigma_{mk}^2.$$

And for $m = M$ the equation reads

$$\left\langle \left| \sum_{j=1}^{2M} \cos(M(\theta_j + \delta\theta_j)) \right|^2 \right\rangle = \left\langle \left| M^2 (2b_{Mk} \sin^2(M\theta_{0k}) + a_{Mk} \sin(2M\theta_{0k})) \right|^2 \right\rangle = M^4 \left(4b_{Mk}^2 \frac{3}{8} + a_{Mk}^2 \frac{1}{2} \right) = 2M^4 \sigma_{Mk}^2.$$

The described ‘‘shot noise’’ algorithm is based on small variations in the longitudinal positions of the macroparticles. Alternatively a variation in the charge can be used as it is described in [13].

Integration of Equations of Motion

The longitudinal equations are discretized with ‘‘leap-frog’’ scheme

$$\begin{aligned} \frac{\psi_{i,j+0.5} - \psi_{i,j-0.5}}{\Delta z} &= \hat{\eta}_{ij} + \hat{C}_j - \frac{B}{2} (\hat{x}_{ij}^2 + \hat{y}_{ij}^2), \\ \frac{\hat{\eta}_{i,j+1} - \hat{\eta}_{i,j}}{\Delta z} &= \frac{\hat{u}_{j+1} + \hat{u}_j}{2} + \left[\psi_{i,j+0.5} + \frac{\varphi_{j+1}^s + \varphi_j^s}{2} \right] + \hat{E}_{z,j+0.5}, \end{aligned}$$

and for the transverse equations a matrix formalism of the linear beam optics is applied

$$\begin{aligned} \begin{pmatrix} \hat{x}_{i,j+1} \\ \hat{x}'_{i,j+1} \end{pmatrix} &= M_x \begin{pmatrix} \hat{x}_{i,j} \\ \hat{x}'_{i,j} \end{pmatrix}, & i = 1: N_p, j = 1: N_z, \\ \begin{pmatrix} \hat{y}_{i,j+1} \\ \hat{y}'_{i,j+1} \end{pmatrix} &= M_y \begin{pmatrix} \hat{y}_{i,j} \\ \hat{y}'_{i,j} \end{pmatrix}. \end{aligned}$$

Solution of the Parabolic Field Equation

The transverse mesh is constructed in polar coordinates with N_r divisions along the radius and N_φ divisions along the angle. Each slice is tracked through the undulator with N_z periods. In the following we consider time-independent case and only later on we will discuss the general case.

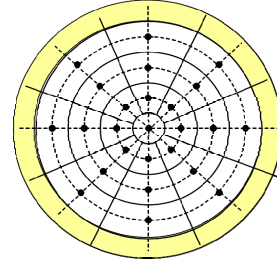


Figure 2: The transverse mesh with PML.

To find the transverse field we use the Fourier transform in azimuthal coordinate. For each azimuthal mode m we have to solve the parabolic equation (in a simplified notation)

$$\left[\frac{1}{2iB} \frac{1}{r} \frac{\partial}{\partial r} r \frac{\partial}{\partial r} - \frac{m^2}{r^2} + \frac{d}{dz} \right] u^{(m)} = -2a^{(1)(m)}, r \in (0, \infty),$$

with the condition on the axis

$$\frac{\partial}{\partial r} u^{(0)}(0) = 0, u^{(m)}(0) = 0, m > 0.$$

In order to truncate the mesh at radius r_0 we use an absorbing layer called Perfectly Matched Layer (PML) [14], which possesses the desired property of generating very low numerical reflection. In order to construct a mathematical model of the PML we introduce the complex variable

$$\tilde{r} = r + \frac{i}{B} \int_0^r \sigma(\xi) d\xi, \quad \sigma(r) = \begin{cases} 0, & r \leq r_0 \\ \geq 0, & r > r_0 \end{cases}.$$

The change of the variable r to \tilde{r} (and the partial derivative $\partial/\partial r$ to $\partial/\partial \tilde{r}$) in the parabolic wave equation will give us the required equation. This change of variable does not alter the solution in the area of interest ($r < r_0$), but it extends the solution by a fast exponentially decaying part in the absorbing layer $r_0 < r < r_{PML}$.

Let us introduce the radial mesh

$$\tilde{r}_j = \tilde{r}_{j-1} + \frac{i}{B} \sigma_{j-0.5} \Delta r, \quad j = 1: n_r, n_r = r_0 / \Delta r,$$

$$\sigma_{j-0.5} = \begin{cases} 0, & j \leq \tilde{n}_r, \\ B \frac{10}{\Delta r} \left(\frac{r_{j-0.5}}{L_{PML}} \right)^2, & \end{cases}$$

$$r_{j-0.5} = (j - n_r - 0.5)\Delta r, \quad L_{PML} = r_{PML} - r_0.$$

The implicit Neumann numerical scheme reads

$$c_q u_{q+1}^{n+1} + b_q u_q^{n+1} + a_q u_{q-1}^{n+1} = f_q^n,$$

$$c_q = \frac{\Delta z}{4iB} \frac{1}{\tilde{r}_j} \frac{\tilde{r}_{j+0.5}}{(\tilde{r}_{j+0.5} - \tilde{r}_{j-0.5})(\tilde{r}_{j+1} - \tilde{r}_j)},$$

$$a_q = \frac{\Delta z}{4iB} \frac{1}{\tilde{r}_j} \frac{\tilde{r}_{j-0.5}}{(\tilde{r}_{j+0.5} - \tilde{r}_{j-0.5})(\tilde{r}_j - \tilde{r}_{j-1})},$$

$$b_q = (1 - a_q - c_q) - \frac{\Delta z}{iB} \frac{m^2}{\tilde{r}_j^2},$$

$$f_q^n = -c_q u_{q+1}^n + (2 - b_q) u_q^n - a_q u_{q-1}^n - 2\Delta z_j a^{(1)}(q).$$

We supply this scheme with the discrete boundary condition at r_{PML}

$$a_{n_r+n_{PML}} = c_{n_r+n_{PML}} = f_{n_r+n_{PML}}^n = 0; \quad b_{n_r+n_{PML}} = 1; \quad m \geq 0,$$

and a discrete boundary condition at $r=0$. The last condition for the monopole mode reduces to

$$c_0 = \frac{\Delta z}{iB} \frac{1}{\Delta r^2}, \quad a_0 = 0, \quad b_0 = 1 - c_0,$$

$$f_0^n = -c_0 u_1^n + (2 - b_0) u_0^n - 2\Delta z a^{(1)}(0),$$

and for higher order modes it reads

$$a_0 = c_0 = f_0^n = 0; \quad b_0 = 1; \quad m > 0.$$

Figure 2 sketches the used transverse mesh. The black points present the location of sample points for the field.

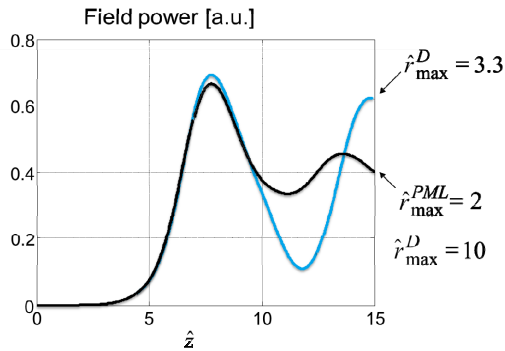


Figure 3: The radiation power with and without PML.

In FEL simulations the Dirichlet boundary condition works satisfactory in the exponential growth regime (linear regime), but it could spoil the correct solution after the saturation (non-linear regime). Figure 3 shows a 3D simulation for a round beam with radius $\hat{r}_b = 1$. It can be seen that for the Dirichlet condition the mesh should be truncated very far from the beam (at $\hat{r}_0 = 10$). On the contrary, the quite thin perfectly matched layer (only 7 mesh points) allows to truncate the mesh accurately already at radius $\hat{r}_0 = 2$.

Time-dependent Simulations

Let us consider the time-dependent equation along the trajectory $t = t_0 + z/c$

$$\left[\frac{\nabla_{\perp}^2}{2ik} + \frac{d}{dz} \right] \tilde{E} \left(z, t_0 + \frac{z}{c} \right) = F \left(z, t_0 + \frac{z}{c} \right).$$

We divide the bunch in N_s slices of the length Δs and numerate them from the tail by index j . The slice with index j cross $z=0$ at the moment of time

$$t_{j0} = -\frac{j\Delta s}{c}$$

and it will reach the position z at the time

$$t_j(z) = -\frac{j\Delta s}{c} + \frac{z}{v_z}.$$

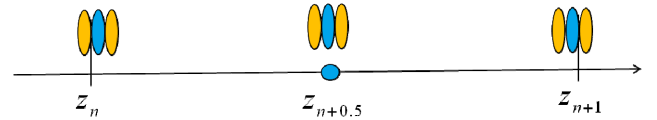


Figure 4: Time-dependent case.

The derivative in z can be approximated as

$$\frac{d}{dz} \tilde{E} \left(z_{n+0.5}, t_j(z_{n+0.5}) \right) =$$

$$= \frac{\tilde{E} \left(z_{n+1}, t_j(z_{n+0.5}) + \frac{0.5\Delta z}{c} \right) - \tilde{E} \left(z_n, t_j(z_{n+0.5}) - \frac{0.5\Delta z}{c} \right)}{\Delta z} + O(2)$$

Let us consider Figure 4 and derive the following relations

$$t_j(z_{n+0.5}) + \frac{\Delta z}{2c} = -\frac{j\Delta s}{c} + \frac{z_{n+0.5}}{v} + \frac{\Delta z}{2c} =$$

$$= -\frac{(j+0.5)\lambda}{c} + \frac{z_{n+1}}{v} = t_{j+0.5}(z_{n+1}),$$

$$t_j(z_{n+0.5}) - \frac{\Delta z}{2c} = t_{j-0.5}(z_n).$$

Hence we can write

$$\frac{\nabla_{\perp}^2}{2ik} \left(\frac{\tilde{E}_{n+1}^j + \tilde{E}_n^{j-1}}{2} \right) + \frac{\tilde{E}_{n+1}^j - \tilde{E}_n^{j-1}}{\Delta z} = F(z_{n+0.5}, t_j(z_{n+0.5})),$$

where

$$\tilde{E}_n^j = \tilde{E} \left(z_n, t_{j+0.5}(z_n) \right)$$

means the EM field of slice j at position z_n .

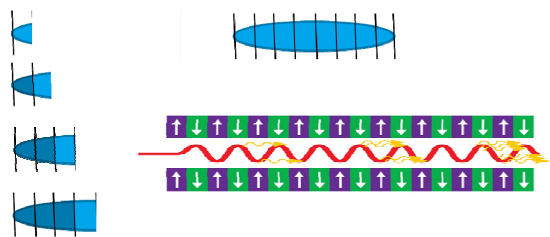


Figure 5: Parallelization.

It follows from the last equation that the field of slice j at position z_n can be found easily if we know the field of the previous slice $j-1$ at the previous position z_{n-1} . Hence the above described algorithm can be parallelized as sketched in Figure 5. We start from the last slice and track the particles of this slice through the whole undulator; the radiated EM field is saved. Then we track the next slice in the radiation field of the previous slice and so on. The three codes listed in Table 1 are parallelized and show the linear scaling of performance in proportion to the number of processes used.

NUMERICAL EXAMPLE

Expected Radiation in the FLASH with 3rd Harmonic Module

In order to linearize the energy chirp before the first bunch compressor the third harmonic module is installed in FLASH at the end of 2009.

To find working points, to define the tolerances and to characterize the parameters of the bunch at the undulator entrance we have done series of “start-to-end” simulations for different bunch charges [15].

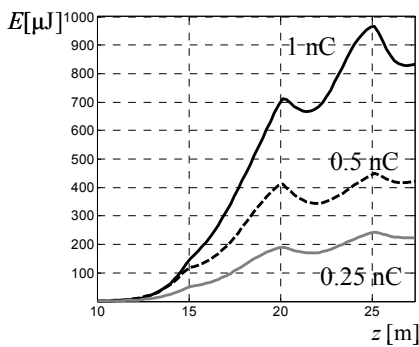


Figure 6: Radiation energy at FLASH.

Figure 6 presents the evolution along the undulator of the radiation energy in SASE mode for different bunch charges. The full set of plots for different characteristics of the obtained radiation can be found in [16].

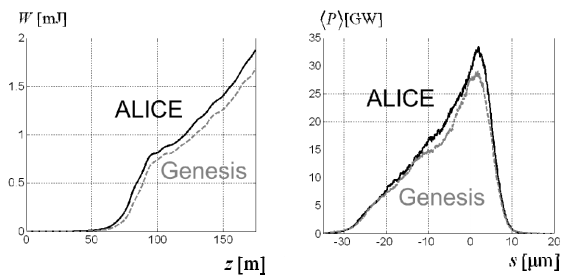


Figure 7: Radiation energy at the European XFEL.

Figure 7 presents comparison of two codes for the set of parameters of the European XFEL [16] as well.

OUTLOOK

The approximations used in the described FEL model allow studying of many features of the physical processes in undulators. The existing FEL codes are benchmarked by comparison with experiments [17] and with analytical results [7]. However for certain problems such as space charge dominated beams, ultra short electron beam pulses, high diffraction cases the used approximations begin to fail and numerical solution of the original set of Maxwell-Vlasov set of equations is required. There are several codes [18, 19] where non-averaged equations of motion are used, but the field is found from the paraxial approximation in the same manner as described in this paper. Abandoning of the paraxial approximation (slowly-varying envelope approximation) will result in necessity to use quite time consuming models as, for, example PIC model. A promising approach for the PIC simulations could be the approach based on Lorentz-boosted frame transformation [20, 21].

REFERENCES

- [1] T.M. Tran, J.S.Wurtele, Phys. Reports 195 (1990) 1
- [2] E.L.Saldin et al, NIM A 429 (1999) 233.
- [3] S. Reiche, NIM A 429 (1999) 243.
- [4] W.M. Fawley, LBNL CBP Tech Note-104 (1995).
- [5] I.Zagorodnov, M.Dohlus, Numerical Studies with a New Code ALICE, FEL 2009, Malmö, 2009, MOPC16.
- [6] S.Reiche, FEL Simulations: History, Status and Outlook, FEL 2009, Malmö, 2009, MOOC11.
- [7] E.L. Saldin et al, The Physics of Free Electron Lasers, Springer (1999).
- [8] J.M.Dawson, Rev. of Modern Physics 55 (1983) 403.
- [9] W.H.Press et al, Numerical Recipes in C, Cambridge University Press (1988).
- [10] The European X-Ray Free Electron Laser TDR, DESY 2006-097 (2006).
- [11] I.Zagorodnov, Genesis/ALICE benchmarking (2008), http://www.desy.de/xfel-beam/talks_a.html#
- [12] W.M. Fawley, Phys. Rev. STAB 5 (2002) 070701.
- [13] B.W.J. McNeil et al, PR STAB 6, (2003) 070701.
- [14] F. Collino, J. Comp. Phys. 131 (1997) 164.
- [15] Zagorodnov I., Dohlus M., PR STAB 14 (2010) 014403.
- [16] Zagorodnov I., Ultra-short low charge operation at FLASH and the European XFEL, FEL 2010, Malmö, Sweden, 2010, WE0B12.
- [17] L. Giannessi et al, PR STAB 14 (2011) 060712.
- [18] H.P. Freund et al, IEEE J.Quantum Electron. 36 (2000) 275.
- [19] C.K.W.Nam et al, Unaveraged Three-Dimensional Modelling of the FEL, FEL 2008, Gyeongju, Korea, MOPPH025.
- [20] J.-L. Vay, PRL 98 (2007) 130405.
- [21] W.M.Fawley, J.-L.-Vay, Full Electromagnetic FEL Simulation via the Lorentz-Boosted Frame Transformation, FEL 2010, Malmö, Sweden, 2010, MOPB01.